International Journal of Research in Engineering and Innovation (IJREI)

Home page http//: www.ijrei.com

Analysis of Vortex Formation around a Circular Cylinder at low Reynolds Number

Vipul Namdev, Prashant Kumar, Ashish Tyagi, Kartik Kumar

Graduate Student, Department of Mechanical Engineering, Meerut Institute of Technology, Meerut, India

Keywords

Reynolds Number,
Lift coefficient
Drag coefficient
Circular Cylinder
Angle of attack

Abstract

Vortex shedding is one of the most interesting phenomenon in turbulent flow. This phenomenon was first studied by Strouhal. In this paper, the analysis of vortex shedding around a 2 dimensional circular cylinder with Reynolds No of 200, 500, and 1000 with different angle of attack 0^0, 5^0, and 10^0 has been studied. In this simulation an implicit pressure-based finite volume method and second order implicit scheme is used. Flow has been studied with the help of Navier-Stokes and continuity equations. The pressure, drag coefficients and vortex shedding for different Reynolds numbers and different angle of attack were computed and compared with other numerical result that show good agreement.

© 2016 ijrei.com. All rights reserved

1. Introduction

The effect of the flow over a rotating cylinder at high rotational rates. 12 rotational rates from 0 to 8 are examined at 3 Reynolds number, Re = 5×10^5 ,10^6 and 5×10^6 . This study shows that the lift and drag force varies slightly in the Reynolds number range (less than 10%). Lift increases linearly with spin ratio (a) and the drag force increases up to a = 4, where it reaches a plateau and eventually decreases. [1].

Investigate high Reynolds number flow (1×10^6 , 2×10^6 , 3.6×10^6) around a smooth circular cylinder by using 2D URANS equation with a standard K-epsilon turbulence model for engineering applications in the supercritical and upper-transition flow regimes was examined in this research. The essential hydrodynamic quantities such as coefficient of drag, lift and strouhal number predictions shows acceptability of the data. The computed cd and skin friction coefficient decrease slightly as the Reynolds number increase [2].

The deflection is increased when we increased the Reynolds Number with increase their angle of attack The maximum deflection occur in Re-1000, angle of attack 15^0 i.e. 9.2597×10^{-3}mm and minimum value of deflection occurs in Re-100 with angle of attack 0^0 i.e.1.4618×10^{-4} mm. the highest natural frequency 34.353 Hz was found in mode 6 which is torsional mode, whereas minimum natural frequency 0.6951 was found in mode [3].

The time-averaged lift and drag generation of two flexible membrane wings with different skin flexibilities (flexible nylon and flexible latex wings) are compared with those of a rigid wing.The effect of the Reynolds number on the gliding ratio is that at Re 1000 and at angle of attack (here after, AOA) 15^0 , the largest gliding ratios are obtained. Flow invariably for all Reynolds number, minimum Drag coefficient is obtained at AOA 15^0 [4]

It was found that for all the simulations performed flow always remained steady at Re 100 and 200 at all angle of attack (0^0 to 15^0). First unsteady flow was obtained at Re 500 and AOA 10^0 . But flow always remained steady at AOA 0^0 and 5^0 for all the Reynolds numbers [5].

The mean drag coefficient is under predicted by this method for a wide range and strouhal number is over predicted. The length of separation bubble predicted shown

Corresponding Author: Vipul Namdev
Email address: Vipulnamdev1995@gmail.com
Copyright ©ijrei.com

good agreement with two layer RSE model. The mean velocity distribution along the center line behind cylinder by this analysis yield fair agreement with experiment but pressure drop curve is unrealistic due to over prediction of the horizontal velocity at the boundary of the wake. So this classical K-ε model with wall law for unsteady turbulent flow is not satisfactory [6].

K-ε model for numerical prediction of long time average flow over circular cylinder at high Reynolds number (10^4 – 10^7). In subcritical region, the transitional model is used and all predictions such as pressure distribution, wall shear stress, and velocity field shows fair agreement with the other results up to the separation point but thin boundary layer should have fine grid. This research suggests using fine grid near the cylinder to obtain fine results. So K-ε model with transition works well for this type of flow [7].

The effect of variation in inlet turbulence length scale on the flow properties by Kω- SST model at Re = 1.4×10^5 and investigate the acceptability of modified time limit K-ω model. The modification in turbulent viscosity term prevents production of turbulent kinetic energy in highly strained area. The performance of CFD is poor in capturing the effect of boundary condition variations, and it is evident that improvements in eddy-viscosity modeling are required. The time limit model is examined at Re = 10^3 to 3×10^6 and the result shows that this model predict more closely than standard model upto 5×10^5 [8].

Applicability of LES for high Reynolds number (Re = 140,000) subcritical flow over circular cylinder and investigate the effect of dynamic subgrid scale (SGS) modeling and Smagorinsky model at different grid on the predicted result. This study shows that dynamic model works well for complex flow at higher Re and grid refinement does not improve the prediction quality due to dependency of the filter width from the grid resolution [9].

A number of roughness pattern are investigated in BLWT at Reynolds number from $1\text{x}10^4$ to $2\text{x}10^5$. The simulations performed by using a large eddy simulation (LES) at high Re ($1.5\text{x}10^6$) and medium Re ($1\text{x}10^5$) and low Re ($3.0\text{x}10^4$). The pressure coefficient is compared for both the case and it shows that artificial roughness pattern can simulate super critical flow properties in sub critical region. The suitability of roughness pattern for definite flow characteristics is remains for research [10].

Implemented large eddy simulation to predict the effect of spin ratio varying from 0 to 2 on the flow parameters of a rotating cylinder at Re = 1.4×10^5 , lift coefficient increases with spin ratio while the drag coefficient reduces. The negative mean pressure coefficient reduces with spin ratio and its position moves toward lower surface. For spin ratio greater than 1.3, the load stabilized after a transition period and variation in lift coefficient reaches its minimum value [11].

The magnitude of drag coefficient and reciprocal of strouhal number decreases, as the Reynolds number increases. Both shows similar trend as experiment but the value are over predicted. By using special wall function the drag crisis phenomena can be observed. 3d modeling and fine grid can be used for the drag crisis phenomena [12].

The mean coefficient of drag predictions show qualitative trend with over predicted values. The higher drag coefficient is due to the absence of three dimension effect in 2D numerical simulation. The pressure coefficient predictions are acceptable from the front face to the point of separation but at the back face, results are under predicted. All results show the acceptability of mesh free vortex method to simulate complex flow with acceptable accuracy [13].

The flow over the cylinder is at Re =$8\times10^{6.}$ Three grids with coarsest mesh having 1.47×10^6 cells and finest mesh having 9.83×10^6 cells are used for prediction of pressure and force coefficient. The averaged drag coefficient, Strouhal number, coefficient of skin friction and separation angle for each of the grids using DES97 and DDES are in good agreement. The pressure coefficient for both models and each grid are similar [14].

Applied finite-element scheme to a problem of high Reynolds number flows varies from at Re = 10^3 to $l0^6$ past a circular cylinder and investigate the effect of boundary layer subdivision on the flow characteristics. In different subdivisions, the number of nodal points varies in the boundary layer. The predictions with fine subdivision of the boundary layer shows decrement and the recovery of the drag coefficient at high Reynolds numbers. For higher Reynolds numbers than Re = 10^4 , finer subdivisions will be needed for the quantitative analysis and for lower Reynolds number the predictions are same for coarser and finer subdivision of boundary layer. All predictions show that a fine subdivision of the boundary layer was required in order to capture the behavior of the flow at a high Reynolds number [15]

Investigates the turbulent flows past a stationary circular cylinder and past a rigid cylinder undergoing forced harmonic oscillations at Reynolds number Re = 10^4 by direct numerical simulations (DNS). Multilevel - type parallel algorithm with combined spectral-element/Fourier discretization on unstructured grids is used in the simulations. The drag coefficients, lift coefficients and the strouhal number are in good agreement and mean pressure distribution on the cylinder surface with high-resolution mesh agree well with the experimental results [16]

The vortex can cause material removal, or scour, at the base of the cylinder, which can lead to the failure of the pier or bridge pylon. The flow past a circular cylinder is associated with various instabilities. These instabilities involve the wake, separated shear layer and boundary layer. Upto Re=47, the flow is steady with two symmetric vortices on each side of the wake center line [17].

2. Governing Equation

2.1 Fluid Flow

The solver employs a time-dependent, conservative form of the incompressible Navier-Stokes equations discretized with a finite-volume approach. The incompressible Navier-Stokes equations written in tensor form are

$$\frac{\partial U_i}{\partial x_i} = 0 \quad (1)$$

$$\frac{\partial U_i}{\partial t} + \frac{\partial (U_i U_j)}{\partial x_j} = -\frac{1}{\rho}\frac{\partial P}{\partial x_i} + \upsilon \frac{\partial}{\partial x_j}\left(\frac{\partial U_i}{\partial x_j}\right) \quad (2)$$

Where the indices, i = 1, 2, 3, represent the x, y and z directions, respectively; and the velocity components are denoted by U_1, U_2, and U_3 corresponding to U, V, W respectively. The equations are non-dimensionalized with the appropriate length and velocity scales, The Navier-Stokes equations are discretized using a cell-centered, non-staggered arrangement. In addition to the cell-center velocities, the face-center velocities are computed and used for calculating the volume flux of each cell. The tensor equations in (2) are written as

$$\frac{\partial u_i}{\partial t} + \frac{\partial (u_i u_j)}{\partial x_j} = -\frac{\partial p}{\partial x_i} + \frac{1}{Re}\frac{\partial^2 u_i}{\partial x_j \partial x_j} \quad (3)$$

$$\frac{\partial u_i}{\partial x_i} = 0 \quad (4)$$

Where Re corresponds to the Reynolds number and is defined as

$$Re = \frac{\rho U_o c}{\mu} \quad (5)$$

Here, ρ and μ are density and dynamic viscosity of the fluid.

2.2 Pressure Velocity Coupling

2.2.1 Simple Algorithm

The SIMPLE algorithm uses a relationship between velocity and pressure corrections to enforce mass conservation and to obtain the pressure field.

If the momentum equation is solved with a guessed pressure field p*, the resulting face flux j_f^*, computed as

$$j_f^* = \hat{j}_f^* + d_f(p_{co}^* + p_{c1}^*) \quad (6)$$

does not satisfy the continuity equation. Consequently, a correction j_f' is added to the face flux j_f^*

$$j_f = j_f^* + j_f' \quad (7)$$

So that the corrected face flux satisfies the continuity equation. The SIMPLE algorithm postulates that j_f' be written as

$$j_f' = d_f(p_{co}' + p_{c1}') \quad (8)$$

where p' is the cell pressure correction

The Simple algorithm substitutes the flux correction equations (Equations 7 and 8) into the discrete continuity equation to obtain a discrete equation for the pressure correction p' in the cell

$$a_p p' = \sum_{nb} a_{nb} p_{nb}' + b \quad (9)$$

where the source term b is the net flow rate into the cell

$$b = \sum_f^{N_{faces}} J_f^* A_f \quad (10)$$

The pressure-correction equation (Equation 9) may be solved using the algebraic multigrid (AMG) method. Once a solution is obtained, the cell pressure and the face flux are corrected using

$$p = p^* + \alpha_p p' \quad (11)$$

$$J_f = J_f^* + d(p_{co}' - p_{c1}')$$

Here α_p is the under-relaxation factor for pressure. The corrected face flux J_f, satisfies the discrete continuity equation identically during each iteration.

3. Boundary Condition

The grid is divided into two regions as shown in figure. A constant velocity u=2 m/sec is imposed on the left side of grid, and the right side set as an outflow region where the gradient values are set to zero. The components are taken in accordance with the angle of attack. Pressure on the both sides was taken as atmospheric i.e. $P=P_{atm}$

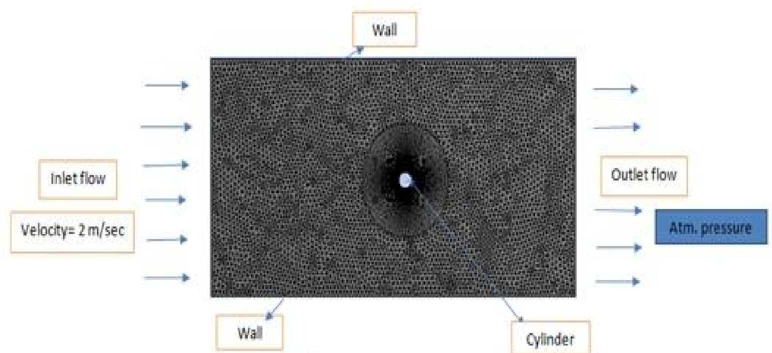

Figure 1: Meshing of the problem

4. Result and Discussion

In this work, around nine simulations were performed in order to see the effect of Reynolds number and angle of attack on circular cylinder and calculate global properties like Drag coefficients, pressure distribution and vortex shedding.

4.1 Validation

The present simulation were carried out at Re=200, 500 and 1000 at angle of attack 0^0, 5^0, and 10^0. Validation study was carried for Re-200 at angle of attack 0^0. The coefficient of drag C_d is tabulated in table 1. These results are compared with Rajani B.N (2009) which is computational results [18].

Table 1:- Comparison of Drag Coefficient from Rajani [18]

C_d

Reynolds Number	Rajni B N [18]	Present Value
200 at AOA= 0	1.3065	1.297

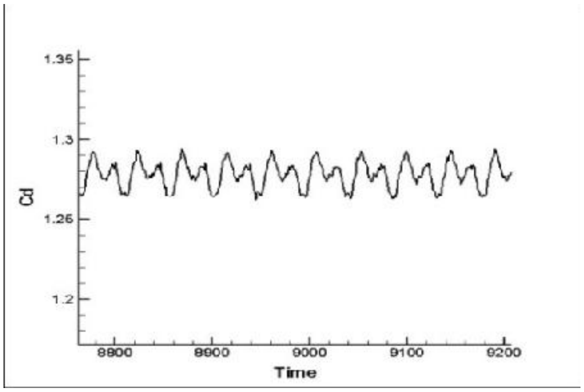

(a)

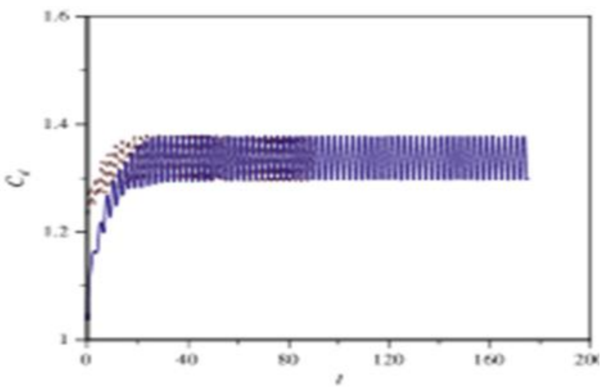

(b)

Figure 2:- Variation of mean drag coefficient and time, (a) Present *Value (b) Rajani B.N et al [18*]

4.2 Simulation Result

In the present study, a computation has been carried out for two-dimensional flow past a circular for Reynolds number varying from 200 to 1000 at angle of attack 0^0, 5^0, and 10^0. The drag force is a result of the convective motion of the cylinder through the fluid. Because of this motion and of the non-slip condition of the wall, a pressure gradient is created in the direction normal to the wall. The mean value of the drag coefficient calculated by the present.

From figure 3-6, it is clearly visible that for Re=200, 500, 1000 the mean drag coefficient decreases, with increasing angle of attack and reynolds numbers, while pressure is increased with increasing reynolds numbers and angle of attack. It can be seen that the largest mean drag cofficient is always obtained at Re-200 with AOA-0^0 and lowest drag coefficient is obtained at Re-1000 with AOA-15^0.

4.2.1 Analysis of Vortex Shedding

Beyond a critical range of Reynolds number of 180–200, the measurement as well as numerical simulation data demonstrate the susceptibility of the two-dimensional wake behind the cylinder to a three-dimensional instability mechanism [19] which amplifies the three dimensional disturbances and eventually leads to the formation of strong stream wise-oriented vortex structure.

The vortex shedding becomes more complicated due to the strong interaction between the body of the cylinder and the surrounding fluid. This interaction causes the development of big vortices on the cylinder as well as the occurrence of the coalescence phenomenon in the near wake region as shown in Figure 7-9.

Such discrepancies have been explained earlier by Mittal and Balachandar [20] as the extraction of energy of the two-dimensional shedding motion by the three-dimensional vertical structures of the flow. This eventually leads to a reduction of the two-dimensional Reynolds stresses which, in turn, increases the base pressure and hence reduces the mean drag

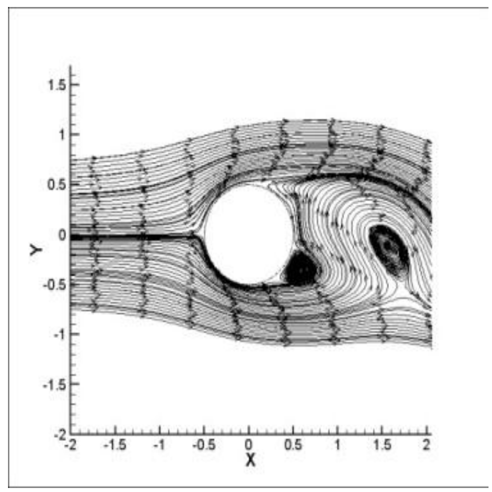

(a)

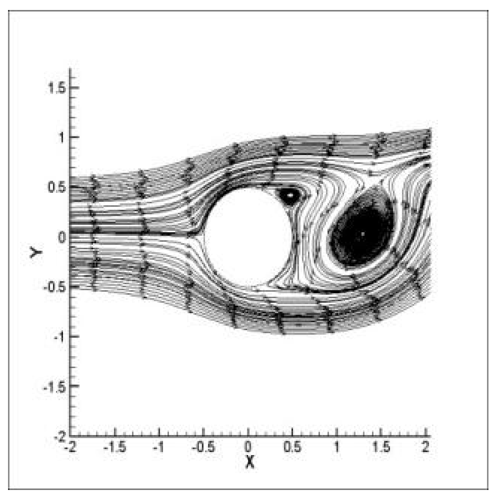

(b)

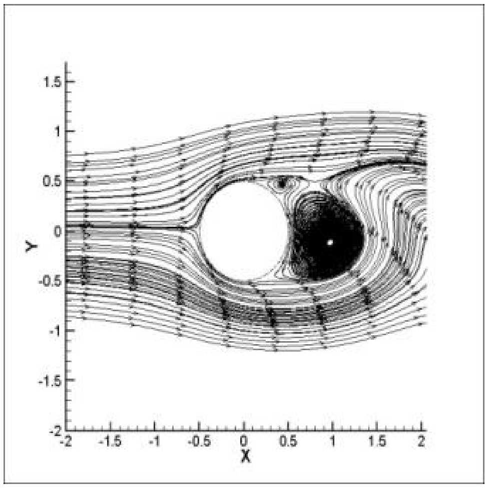

(c)

Figure 7:- Streams lines at Re = 200 for (a) α= 0^0, (b) α= 5^0, (c) α= 10^0

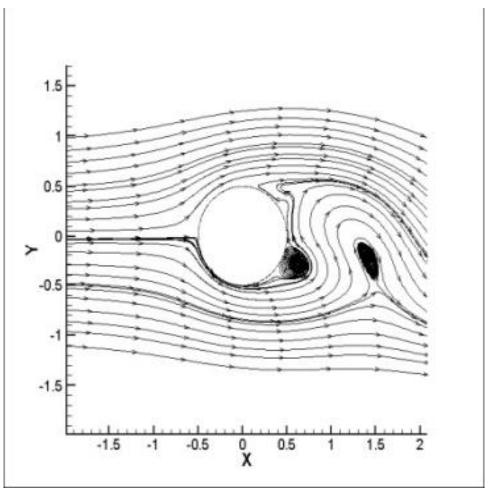

(a)

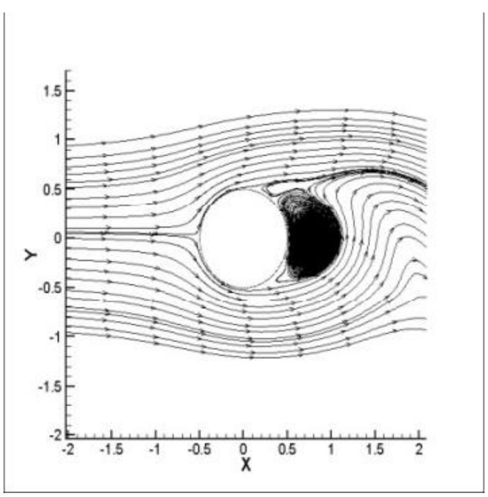

(b)

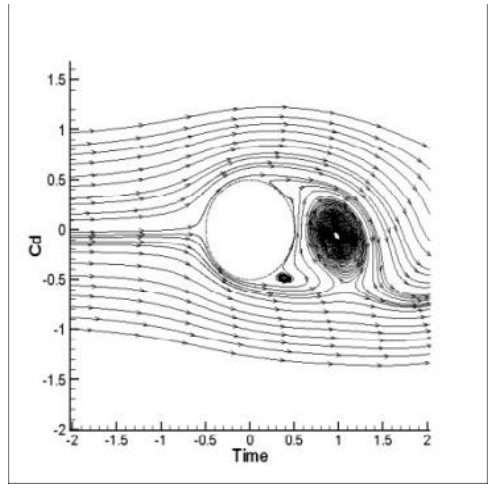

(c)

Figure 8:- Streams lines at Re = 500 for (a) α= 0^0, (b) α= 5^0, (c) α= 10^0

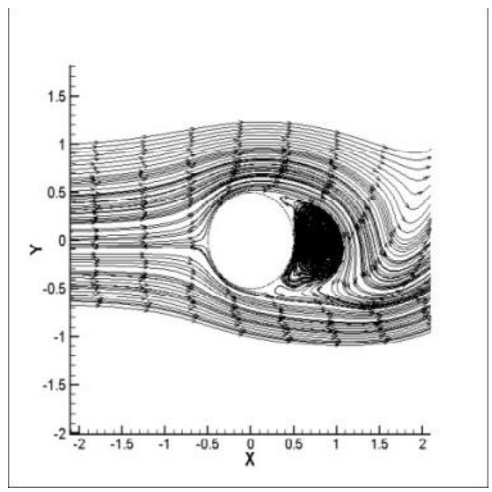

(a)

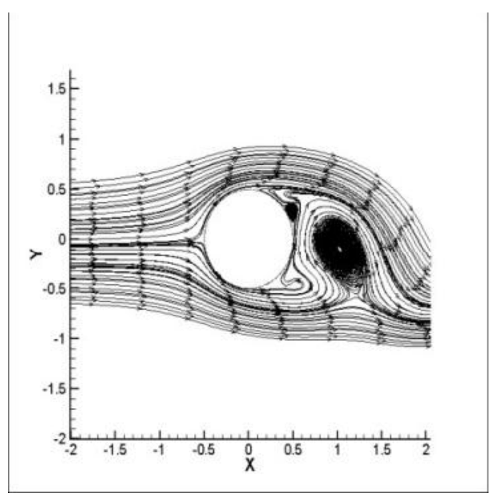

(b)

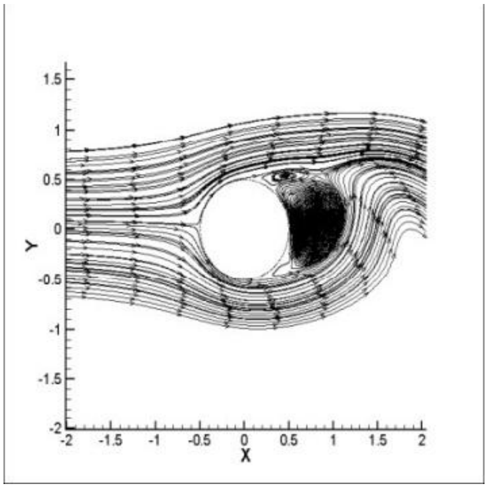

(c)

Figure 9:- Streams lines at Re = 1000 for (a) α= 0^0, (b) α= 5^0, (c) α= 10^0

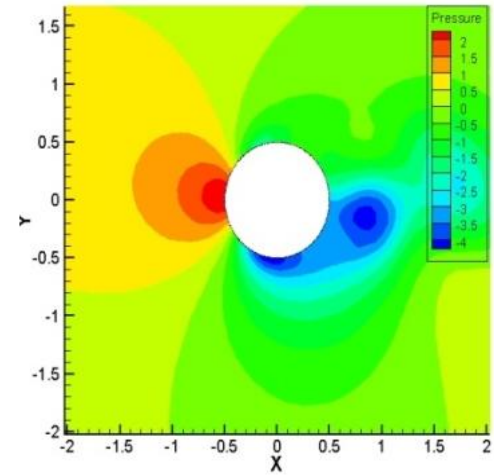

(c)

Figure 10:- Pressure contours at Re = 200 for (a) α= 0^0, (b) α= 5^0, (c) α= 10^0

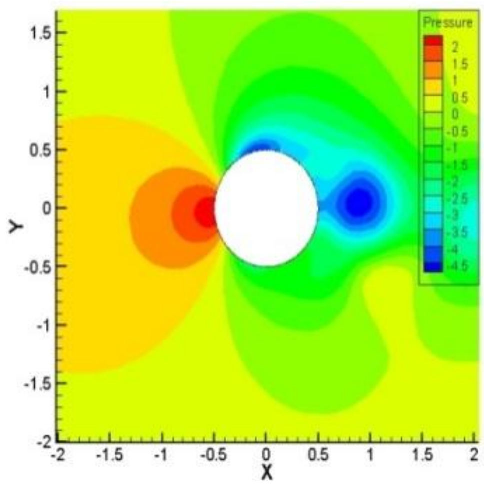

(a)

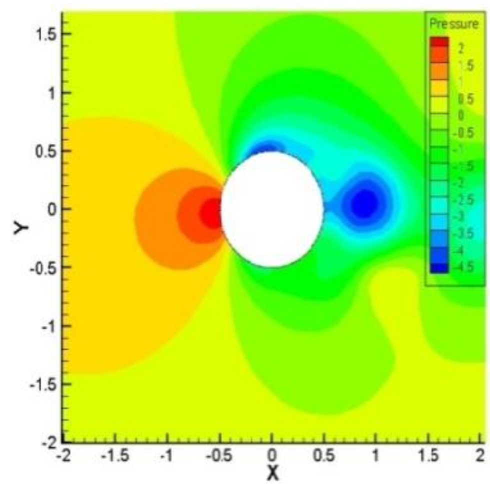

(a)

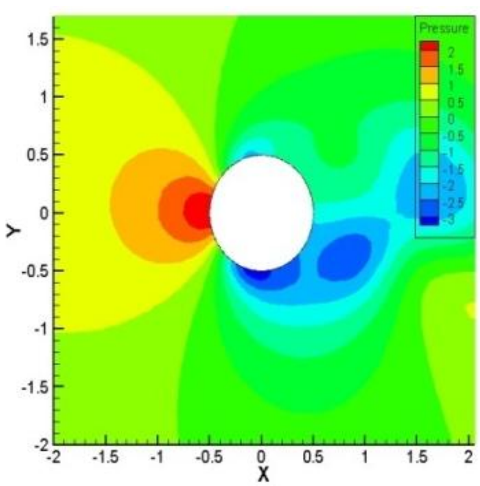

(b)

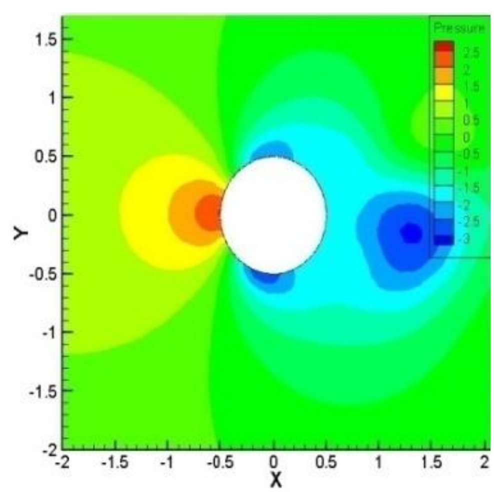

(b)

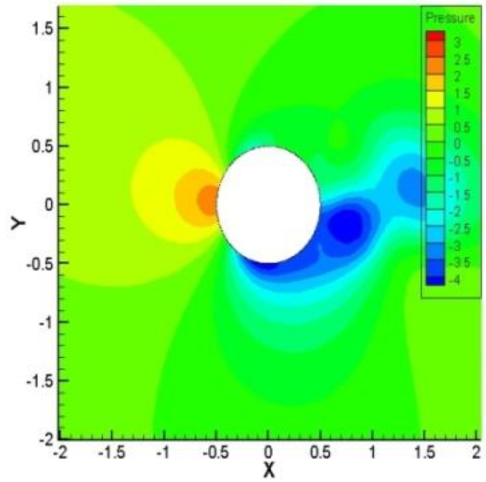

(b)

Figure 11:- Pressure contours at Re = 500 for (a) α= 0⁰, (b) α= 5⁰, (c) α= 10⁰

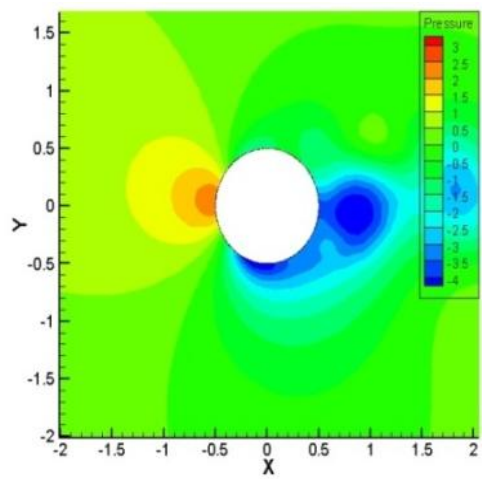

(a)

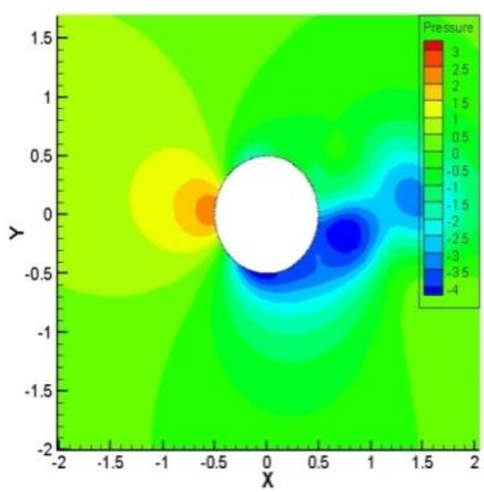

(b)

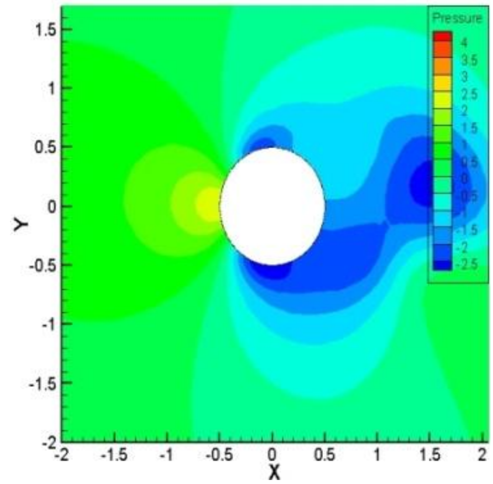

(c)

Figure 12:- Pressure contours at Re = 1000 for (a) $\alpha= 0^0$, (b) $\alpha= 5^0$, (c) $\alpha= 10^0$

The basic step in understanding the drag coefficient and pressure at Reynolds number of 200, 500 and 1000 was to analyse the flow at 0^0, 5^0, 10^0 angle of attack. The mean force coefficients and pressure are tabulated in table 2. The drag production leads to some interesting observations. As expected, the overall drag coefficient increases with decrease in Reynolds number, because the viscous effects are more dominant at lower Reynolds numbers which cause the skin friction to be the major contributor to the overall drag. As the angle of attack increased, drag coefficient further decreases.

As the angle of attack increases, drag force continue to decrease while lift force continuously increases. This is due to a larger attached vortex on the upper surface of the cylinder. The decrease in drag is due to lower shear drag as the strength of the trapped vortex in the cylinder. As the angle of attack is increased, thus the pressure is larger at the upper side of cylinder and hence an increase in lift is obtained and decrease in drag.

5. Conclusion

In this work, we analyze the fluid flow around a circular cylinder at low Reynolds numbers (200, 500, and 1000) at different angle of attacks 0^0, 5^0, and 10^0.

There are around 9 simulations were performed and the main conclusions are as given below

- The overall drag coefficient increases as Re is decreased. Because the viscous effects are more dominant at lower Reynolds numbers which cause the skin friction to be the major contributor to the overall drag. As the angle of attack is increased, drag coefficient further decreases.
- The mean pressure is increased when Reynolds number and angle of attack increased.
- The flow patterns are found to be unsteady at Reynolds Number 200, 500 and 1000 with angle of attack 0^0, 5^0, and 10^0.

References

[1] S.J. Karabelas, B.C. Koumroglou, C.D. Argyropoulos, N.C. Markatos, “High Reynolds number turbulent flow past a rotating cylinder,” Applied Mathematical Modelling 36, pp. 379–398, 2012.

[2] M.C. Ong, T. Utnes, L.E. Holmedal, D. Myrhaug, B. Pettersen, “Numerical simulation of flow around a smooth circular cylinder at very high Reynolds numbers,” Marine Structures 22, pp. 142–153, 2009.

[3] Husain Mehdi, Fahad Anwer, Akhlaque Ahmad, ”Fluid Structure Interaction of Flow around a Pleated Insect 2D Airfoil at Ultra Low Reynolds Numbers” International Journal of Research in Aeronautical and Mechanical Engineering, vol.3, issue 3, pp 19-37, 2015.

[4] Fahad Anwer “ On the Aerodynamic Performance of Dragon fly wing Section in Gliding Mode” Advances in Aerospace Science and Applications, Vol. 3, pp 227-234, 2013.

[5] Husain Mehdi, Brajesh Kumar, Anil Kumar, “Numerical Analysis of Steady and Unsteady Flow for Dragonfly Wing Section in Gliding Mode” International Journal of Advanced Mechanical Engineering, Vol.4, pp 365-370, 2014.

[6] B. Mohammadi and G. Medic, “A Critical Evaluation of the Classical k-ε " Model and Wall-Laws for Unsteady Flows over Bluff Bodies

[7] I. Celik , F.D. Shaffer, “Long time averaged solutions of turbulent flow past a circular cylinder,” Journal of Wind Engineering and Industrial Aerodynamics 56, pp. 185–212, 1995.

[8] M. E. Young and A. Ooi, “Turbulence Models and Boundary Conditions for Bluff Body Flow,” 15th Australasian Fluid Mechanics Conference The University of Sydney, Sydney, Australia 13-17 December 2004.

[9] M. Breuer, “A challenging test case for large eddy simulation: high Reynolds number circular cylinder flow,” International Journal of Heat and Fluid Flow 21, pp. 648-654, 2000.

[10] R. Merrick and G. Bitsuamlak, “Control of flow around a circular cylinder by the use of surface roughness A computational and experimental approach”.

[11] S.J. Karabelas, “Large Eddy Simulation of high-Reynolds number flow past a rotating cylinder,” International Journal of Heat and Fluid Flow 31, pp. 518–527, 2010.

[12] R.P. Selvam, “Finite element modeling of flow around a circular cylinder using LES,” Journal of WindEngineering and Industrial Aerodynamics 67 & 68, pp. 129–139, 1997.

[13] A.A. Mustto and G.C.R. Bodstien, “Subgrid scale modeling of turbulent flow around circular cylinder by mesh free vortex method,” Engineering applications of computational fluid mechanics Vol. 5, No. 2.pp. 259-275, 2011.

[14] K.D. Squires, V. Krishnan, J.R. Forsythe, “Prediction of the flow over a circular cylinder at high Reynolds number using detached-eddy simulation,“Journal of Wind Engineering and Industrial Aerodynamics 96, pp. 1528–1536, 2008

[15] M. Tabata and S. Fujima, “Finite-element analysis of high Reynolds number flows past a circular cylinder,” Journal of computational and Applied Mathematics 38, pp. 411-424 North-Holland, 1991.

[16] S. Dong, G.E. Karniadakis, “DNS of flow past a stationary and oscillating cylinder at Re = 10000,” Journal of Fluids and Structures 20, pp. 519–531, 2005.

[17] C.H.K. Williamson. Vortex dynamics in the cylinder wake. Annual Review of Fluid Mechanics, 28:477{539, 1996.

[18] B.N. Rajani et al, “Numerical simulation of laminar flow past a circular cylinder”, Applied Mathematical Modelling, pp 1228-1247, 2009.

[19] S. Manoj Kumar, Numerical Computation of Turbulent Flow Past Bluff Bodies, M.Tech Thesis, Department of Mechanical Engineering, National Institute of Technolgy, Calicut, Kerala, 2004.

[20] R. Mittal, S. Balachandar,”Generation of streamwise vortical structures in bluff body wakes” Phys. Rev. Lett, 75 (5) (1995), pp. 1300–1303.

[21] Husain Mehdi, Fahad Anwer, Akhlaque Ahmad, “Vibration Analysis of Dragonfly wing section in Gliding Mode at Low Reynolds Number” International Journal of Research in Aeronautical and Mechanical Engineering, vol. 2, issue 12, pp 11-23, 2014.